

Fermi Surface Nesting with Heavy Quasiparticles in the Locally Noncentrosymmetric Superconductor CeRh₂As₂

Yi Wu,^{1,*} Yongjun Zhang,^{2,*} Sailong Ju,³ Yong Hu,³ Yanen Huang,¹ Yanan Zhang,¹ Huali Zhang,¹ Hao Zheng,¹ Guowei Yang,¹ Evrard-Ouicem Eljaouhari,⁴ Baopeng Song,² Nicholas C. Plumb,³ Frank Steglich,^{1,5} Ming Shi,^{1,3} Gertrud Zwicknagl,^{4,5} Chao Cao,^{1,†} Huiqiu Yuan,^{1,6,7,‡} and Yang Liu^{1,6,§}

¹*Center for Correlated Matter and School of Physics, Zhejiang University, Hangzhou 310058, China*

²*Institute for Advanced Materials, Hubei Normal University, Huangshi 435002, China*

³*Swiss Light Source, Paul Scherrer Institut, CH-5232 Villigen PSI, Switzerland*

⁴*Institut für Mathematische Physik, 38106 Braunschweig, Germany*

⁵*Max Planck Institute for Chemical Physics of Solids, 01187 Dresden, Germany*

⁶*Collaborative Innovation Center of Advanced Microstructures, Nanjing University, Nanjing 210093, China*

⁷*State Key Laboratory of Silicon Materials, Zhejiang University, Hangzhou 310058, China*

(Dated: June 4, 2024)

The locally noncentrosymmetric heavy fermion superconductor CeRh₂As₂ has attracted considerable interests due to its rich superconducting phases, accompanied by a quadrupole density wave and pronounced antiferromagnetic excitations. To understand the underlying physics, we here report measurements from high-resolution angle-resolved photoemission. Our results reveal fine splittings of the conduction bands related to the locally noncentrosymmetric structure, as well as a quasi-two-dimensional Fermi surface (FS) with strong $4f$ contributions. The FS exhibits nesting with an in-plane vector $(\pi/a, \pi/a)$, which is facilitated by the van Hove singularity near \bar{X} that arises from the characteristic conduction- f hybridization. The FS nesting provides a natural explanation for the observed antiferromagnetic excitations at $(\pi/a, \pi/a)$, which could be intimately connected to its unconventional superconductivity. Our experimental results are well supported by density functional theory plus dynamical mean field theory calculations, which can capture the strong correlation effects. Our study not only provides spectroscopic proof of the key factors underlying the field-induced superconducting transition, but also uncovers the critical role of FS nesting and lattice Kondo effect in the intertwined spin and charge fluctuations.

The recent discovery of heavy fermion (HF) superconductivity ($T_c \sim 0.26$ K) in CeRh₂As₂ has attracted broad interest [1]. The large specific jump at T_c indicates that the Cooper pairs are formed out of the heavy quasiparticles as a result of the Kondo effect [1]. A remarkable field-induced first-order transition within the superconducting phase can be observed for a magnetic field applied along the c axis [1], which was attributed to an even-odd parity transition as a result of the local noncentrosymmetry at the Ce sites [1–10]. Such a parity transition is extremely rare for superconductors. A small interlayer hopping and larger Rashba-like spin-orbit coupling (SOC, as a result of the local noncentrosymmetry) are thought to be essential for the parity transition of superconductivity [1, 3–7, 11]. It is therefore imperative to unravel the electronic structure underlying the peculiar superconductivity, particularly the influences of the interlayer coupling and the locally noncentrosymmetric structure.

Another key question in CeRh₂As₂ is the origin of the observed antiferromagnetic (AFM) fluctuations [12] or order [13], as well as the non-magnetic transition at $T_0 \sim 0.4$ K [1, 14]. Pronounced AFM excitations observed from inelastic neutron scattering (INS) [12] and possible AFM order below T_c inferred from nuclear quadrupole resonance [13] point towards a magnetically driven superconductivity in CeRh₂As₂, similar to other prototypical HF superconductors, such as CeCu₂Si₂ [15, 16] and

CeCoIn₅ [17]. Interestingly, quasi-two-dimensional (2D) magnetic excitations were observed at $q_0 = (\pi/a, \pi/a)$ in INS [12], which is often related to the nesting of Fermi surface (FS). On the other hand, the transition at T_0 is proposed to be an unconventional quadrupole density wave (QDW) based on renormalized band calculations [14, 18], where the nesting of the FS (involving itinerant $4f$ bands) is also necessary. Nevertheless, how the itinerant heavy quasiparticles develop and can account for the coexisting spin and charge fluctuations in CeRh₂As₂ remains an open question [19–21].

Here we report measurements of the quasiparticle dispersion and FS in CeRh₂As₂, from angle-resolved photoemission spectroscopy (ARPES). Although there have been a few theoretical studies on the electronic structure [4, 7, 14, 22, 23], high-resolution ARPES measurement is still lacking. Our experimental results are well supported by state-of-art calculations from density functional theory (DFT) plus dynamical mean-field theory (DMFT), and such a combination allows us to develop a thorough understanding of the relevant physics. Details of crystal growth, characterizations, ARPES measurements and calculations can be found in [24] (see also references [25–35] therein).

CeRh₂As₂ crystallizes in a CaBe₂Ge₂-type tetragonal structure (see Fig. 1(a)): each Ce layer is sandwiched by alternating Rh-As-Rh and As-Rh-As trilayers, which break the local inversion symmetry at the Ce

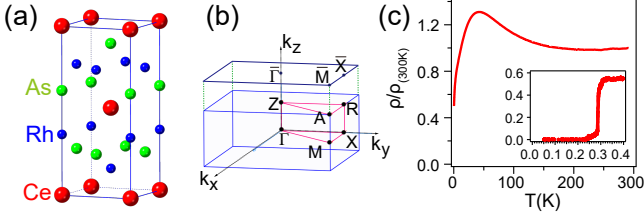


FIG. 1. (a) Crystal structure of CeRh_2As_2 . (b) The bulk (bottom) and projected surface (top) BZ's. (c) Resistivity vs temperature. Inset is a zoomed-in view near T_c .

sites, although the global inversion center still exists. The bulk and surface Brillouin Zone's (BZ's) are displayed in Fig. 1(b). The sample quality is confirmed by the temperature-dependent resistivity (Fig. 1(c)), which exhibits a broad maximum at $T^* \sim 40$ K and a superconducting transition at $T_c \sim 0.24$ K (zero resistivity). Note that the cleaved surfaces for ARPES measurements most likely consist of small domains with different layer terminations, which are smaller than the beam spot (Fig. S2 in [24]). While the mixed surface terminations lead to considerable spectral broadening, they also indicate that the strong features observed experimentally should be bulk states, as verified by comparison with calculations (see below).

Figure 2(a,b) show the dispersion of conduction bands along $\bar{\Gamma} - \bar{M}$ taken with two representative photon energies (additional data and calculations in Fig. S3-S4 of [24]). Except from the flat $4f$ bands at the Fermi level (E_F) and -0.27 eV, which we shall discuss later, the dispersive conduction (non- $4f$) bands well below E_F consist of large electron pockets centered at \bar{M} (denoted as α), as well as both hole (β) and shallow electron (γ) pockets centered at $\bar{\Gamma}$ (blue arrows in Fig. 2(a)). The observed conduction bands away from E_F can be compared reasonably well with the DFT calculations (Fig. 2(c,d)), which treat Ce $4f$ electrons as core electrons (core- $4f$ calculation). For example, the α and β bands show small differences for $k_z = 0$ and $k_z = \pi/c$ (compare Fig. 2(a,c) with Fig. 2(b,d)), and there is a M-shape band near -1 eV at $k_z = 0$ (green dashed circles in Fig. 2(a,c)). The k_z dispersion can be further verified by the photon-energy dependent scan in Fig. 2(e), where the band positions at E_F exhibit weak periodic modulation with k_z , allowing for an estimation of the inner potential $V_0 \approx 15$ eV. Despite some k_z -dependent intensities caused by weak k_z dispersion, the dominant spectral features are nearly vertical and extend along the k_z direction, indicating its quasi-2D nature. The quasi-2D FS implies dominant intralayer hopping compared to the weak interlayer hopping, which is thought to be crucial for the high-field odd-parity superconducting phase in CeRh_2As_2 .

From the DFT calculations, both α and β bands actually consist of two closely spaced (or split) bands, which

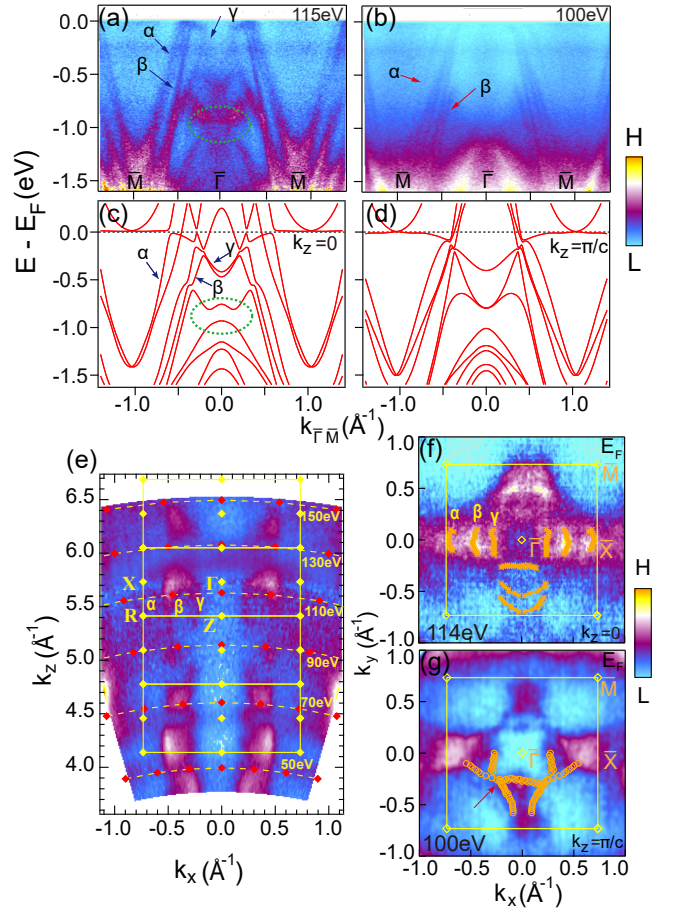


FIG. 2. (a-d) ARPES spectra taken with 115 eV (a) and 100 eV (b) photons along the $\bar{\Gamma} - \bar{M}$ direction, in comparison with DFT calculations at $k_z = 0$ (c) and π/c (d). (e) The k_x - k_z map at E_F along the in-plane $\bar{\Gamma} - \bar{X}$ direction (k_x) using vertically polarized photons. The yellow rectangles (with points) mark the BZ boundaries. Red dashed curves represent various k_z cuts corresponding to different photon energies. (f,g) In-plane FS maps from 114 eV (f) and 100 eV (g) photons. The orange crosses and circles in the lower halves of the FS maps indicate experimentally extracted Fermi contours. The color bars for the image plots are indicated on the right (L: low intensity, H: high intensity).

can be clearly identified in the ARPES data (red arrows in Fig. 2(b)). Direct observation of these fine features demonstrates the high spectral quality. These splittings are closely related to the CaBe_2Ge_2 -type crystal structure, which hosts alternating Rh-As-Rh and As-Rh-As trilayers that break the local inversion symmetry of the Ce layers. Indeed, calculations assuming the ThCr_2Si_2 -type structure with identical As-Rh-As trilayers, where the centrosymmetry of the Ce layers is restored, do not exhibit such band splitting (Fig. S5 in [24]). Therefore, these fine splittings are direct manifestations of the local noncentrosymmetry of the Ce layers, which is intimately connected to the multiple superconducting phases in CeRh_2As_2 [1–10]. We note that for

the HF compounds with the ThCr₂Si₂-type centrosymmetric structure, e.g., CeRu₂Si₂ [36] and CeCu₂Si₂ [37], no similar band splittings have ever been reported.

The in-plane FS maps at $k_z = 0$ and π/c are shown in Fig. 2(f,g), where the Fermi contours extracted experimentally (yellow crosses/circles) are overlaid in the lower halves of the experimental data. For $k_z = 0$ (Fig. 2(f)), the α and β pockets exhibit diamond shape (more discussions below), while the inner γ pocket appears to be square-like. By contrast, at $k_z = \pi/c$ (Fig. 2(g)), the α and β pockets become very close and lead to one large diamond-shaped pocket (highlighted by a red arrow), joined by strong spectral features near \bar{X} .

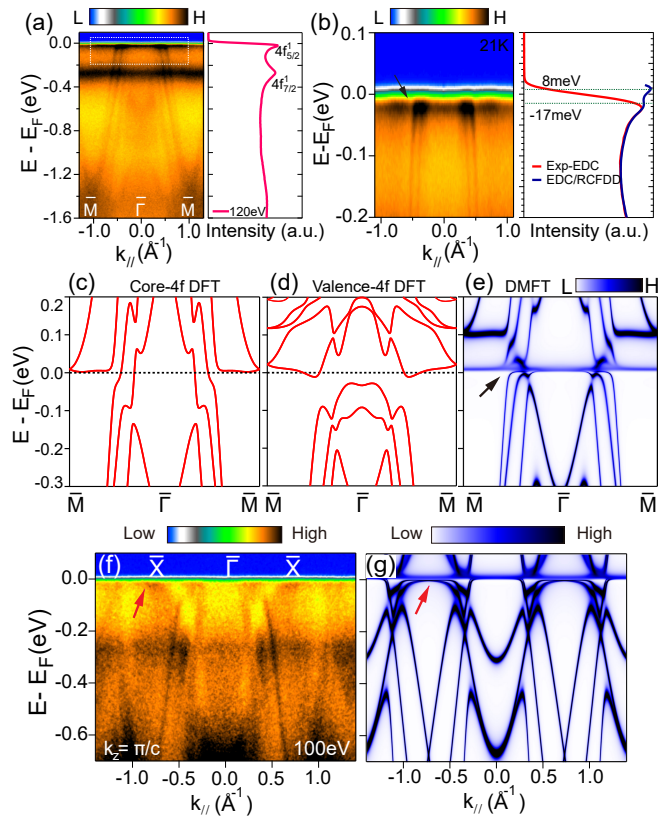


FIG. 3. (a) Resonant ARPES spectra (left) along $\bar{\Gamma} - \bar{M}$ and its corresponding momentum-integrated EDC (right). (b) Zoom-in view of (a) near E_F . Right: the EDC (red) and its division by RC-FDD (blue). The EDCs in (a,b) are integrated from -1.2 to 1.2 \AA^{-1} . (c-e) Band dispersion from core-4f (c), valence-4f (d) DFT calculations and k -resolved spectral function from DFT+DMFT calculations (e), for comparison with (b). The electron-like γ bands at $\bar{\Gamma}$ are not obvious in experiment likely due to small photoemission matrix elements. (f,g) ARPES spectrum along $\bar{\Gamma} - \bar{X}$ at $k_z = \pi/c$ (f), in comparison with DFT+DMFT calculation (g).

Now we discuss the $4f$ states near E_F . We employed resonant ARPES measurement at 120 eV (the Ce N edge), where the photoemission cross section for the $4f$ states near E_F is largely enhanced [38]. The results (Fig. 3(a)) show that the $4f$ states near E_F actually consist of

the $4f_{5/2}^1$ peak near E_F ($J = 5/2$) and the spin-orbit split $4f_{7/2}^1$ peak at $\sim -0.27 \text{ eV}$ ($J = 7/2$), which can be clearly seen in the energy distribution curves (EDCs). These Kondo peaks arise from the many-body Kondo process and develop into propagating heavy bands in a periodic lattice [36, 39, 40]. A zoomed-in view of the quasiparticle dispersion near E_F , as shown in Fig. 3(b), reveals a nearly flat $4f_{5/2}^1$ band and a clear bending of the conduction bands (black arrow), due to hybridization between conduction and $4f$ electrons (c - f hybridization) [41–46]. To compare with experiments, we perform both DFT and DFT+DMFT calculations (Fig. 3(c-e)). Although the core-4f DFT calculation (Fig. 3(c)) can capture the conduction bands away from E_F , it cannot account for the correlated $4f$ bands near E_F . By contrast, the valence-4f calculation (Fig. 3(d)), which treats $4f$ electrons as valence electrons with Hubbard U , can generate $4f$ bands near E_F , but their position and dispersion is very different from experiment - such deviation for the $4f$ bands is not surprising in strongly correlated HF systems. Fig. 3(e) shows the calculated k -resolved spectral function from DFT+DMFT, which reveals very good agreement with experiments: the weakly dispersive $4f$ band and the bending of conduction bands near E_F can be reproduced very well. The bending of conduction bands (black arrows in Fig. 3(b,e)), caused by the c - f hybridization, is also accompanied by an increase of $4f$ weight, leading to characteristic "hot" spots near E_F (Fig. 3(b)). Figure 3(f,g) demonstrate the comparison between ARPES and DFT+DMFT along $\bar{\Gamma} - \bar{X}$ at $k_z = \pi/c$, where excellent agreement can be found. In particular, the heavy hole band near \bar{X} (red arrows in Figure 3(f,g)) gives rise to a van Hove singularity (VHS) at E_F with large density of states (DOS). This VHS, different from the conduction-band VHS at $k_z = 0$ reported in an independent ARPES paper [47], is driven by c - f hybridization characteristic of HF systems (Fig. S3 in [24]).

The unusual QDW at T_0 in CeRh₂As₂ was attributed to mixing of the ground-state and first excited $4f$ doublets due to strong Kondo effect [14], which effectively leads to a quartet ground state for $4f$ electrons, similar to cubic systems with quadrupole order, e.g., CeB₆ [48–50]. Since the crystal electric field (CEF) states of $4f$ electrons can manifest through the fine satellite structures in the Kondo peaks [42, 51–53], we divided the ARPES spectra by the resolution-convoluted Fermi-Dirac distribution (RC-FDD) (Fig. S6 in [24]), which recovers the full spectral function near E_F . The result (right panel in Fig. 3(b)) reveals two $4f$ peaks at $\sim 8 \text{ meV}$ and $\sim 17 \text{ meV}$, respectively. Previous studies suggest that the energy separation between the ground state Γ_7^1 and first excited doublet Γ_6 (second excited doublet Γ_7^2) is $\Delta_1 \sim 2.6 \text{ meV}$ ($\Delta_2 \sim 15.5 \text{ meV}$), respectively [1, 14, 54]. Therefore, the satellite peak at -17 meV could correspond to CEF excitations related to Γ_7^2 , while the peak at $\sim 8 \text{ meV}$

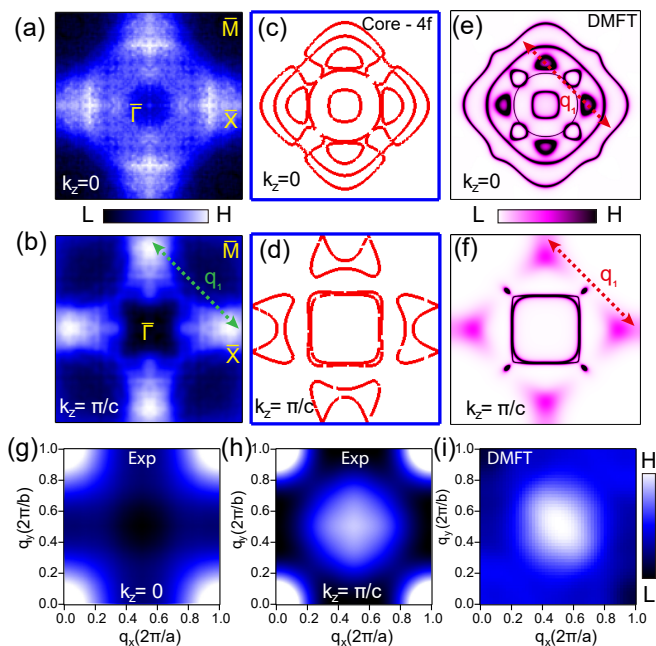


FIG. 4. (a,b) In-plane experimental FS maps within first BZ at $k_z = 0$ (a) and π/c (b). Here the maps are symmetrized according to the bulk C_4 rotation. (c-f) The calculated in-plane FS's from the core- $4f$ DFT (c,d) and DFT+DMFT (e,f) calculations. The dashed arrows in (b,e,f) indicate the nesting vector q_1 . (g,h) Autocorrelation $C(q, 0)$ of the ARPES FS maps for $k_z = 0$ (g) and π/c (h). (i) The quadrupolar susceptibility $\chi(q)$ calculated from DFT+DMFT.

might contain broadened contributions from both Γ_7^1 and Γ_6 , due to limited energy resolution. The observed fine structures of the $4f_{5/2}^1$ Kondo peak, as well as their temperature evolution (Fig. S7 in [24]), are overall consistent with the proposed CEF scheme [1, 14, 54].

Figure 4(a-f) show the detailed comparison between the experimental and theoretical FS's. While the core- $4f$ DFT calculation appears to explain the shape of the experimental FS at $k_z = 0$ (compare Fig. 4(a,c)), it fails to account for the FS at $k_z = \pi/c$ (compare Fig. 4(b,d)). By contrast, the DFT+DMFT calculations in Fig. 4(e,f) show very good agreement with experiments at both k_z cuts, particularly the large diamond-shaped pocket and the strong spectral feature near \bar{X} at $k_z = \pi/c$ (compare Fig. 4(b,f)). Note that the DFT+DMFT FS at $k_z = 0$ has similar shape as the core- $4f$ FS (compare Fig. 3(c,e)), although the pocket sizes are slightly smaller due to band bending from c - f hybridization (Fig. 3(b,e)). Therefore, the experimental FS and its anisotropic $4f$ weight is a direct consequence of the band-dependent c - f hybridization, which is well captured by DFT+DMFT calculations.

Both the experimental and theoretical FS maps exhibit signatures of nesting. A nesting vector $q_1 \approx (\pi/a, \pi/a)$ marked in Fig. 4(b,f) can connect the heavy quasipar-

ticles with high DOS at \bar{X} (see also Fig. 3(f,g)). This vector can also link the parallel portions of the outer α pocket at $k_z = 0$, as indicated by a red dashed arrow in Fig. 4(e). For quantitative analysis of FS nesting, we calculate the autocorrelation $C(q, \omega)$ of the ARPES spectral function $A(\mathbf{k}, \omega)$ via [55–57]

$$C(q, \omega) = \sum_{\mathbf{k}} A(\mathbf{k}, \omega) A(\mathbf{k} + \mathbf{q}, \omega)$$

, where the summation is over the first BZ. The 2D results for the $k_z = 0$ and $k_z = \pi/c$ FS maps are shown in Fig. 4(g,h), respectively. A pronounced peak at $q = (\pi/a, \pi/a)$ in Fig. 4(h) indicates FS nesting at this wave vector. Note that there is no obvious peak at $(\pi/a, \pi/a)$ in the $k_z = 0$ map in Fig. 4(g). This is due to the weak photoemission intensity of the outer α pocket along the diagonal $\bar{\Gamma} - \bar{M}$ direction (see Fig. 4(a)), where large contributions to the FS nesting are expected (red dashed arrow in Fig. 4(e)). The FS nesting can be further verified by the DFT+DMFT calculation in Fig. 4(i), where the quadrupolar susceptibility $\chi(q)$ using the three-dimensional electronic structure obtained from the DFT+DMFT calculation is plotted [24]. The result shows a strong peak at $q = (\pi/a, \pi/a)$, confirming the FS instability associated with this wave vector.

In HF systems, the nesting of FS with heavy quasiparticles is often necessary for the strong magnetic excitations and spin fluctuations [16, 58, 59], which could eventually lead to HF superconductivity. At the nesting vector (usually the same as the AFM ordering vector in parent compound), spin resonances have been detected [59–61], which are closely connected to the superconducting order parameter. Interestingly, the observed FS nesting at $q_1 = (\pi/a, \pi/a)$ in CeRh_2As_2 matches well with the quasi-2D AFM excitations at $(\pi/a, \pi/a)$ from INS measurements [12]. It is therefore desirable to check if spin resonances can be observed at this vector upon entering the superconducting state.

In principle, the proposed QDW at T_0 also requires nesting of the FS [14]. The coexistence of strong magnetic excitations and quadrupole order in CeRh_2As_2 is reminiscent of the famous compound URu_2Si_2 [62], where a "hidden-order" transition at ~ 17.5 K could be attributed to certain type of multipole order [63], accompanied by strong magnetic excitations observed by INS [64–66]. In addition, extensive ARPES studies of URu_2Si_2 revealed partial gapping of the nested FS across the "hidden-order" transition [67–73], although the underlying mechanism remains unsettled. Therefore, CeRh_2As_2 could provide another interesting platform to study the delicate interplay between orbital and magnetic degrees of freedom in correlated f -electron systems, as well as their connection with the unconventional superconductivity [74].

According to theory, a large Rashba-type SOC due to local noncentrosymmetry and a small interlayer

hopping are both crucial for realizing the field-induced parity transition in CeRh_2As_2 [3–7]. Our observation of fine band splittings caused by the locally noncentrosymmetric structure (Fig. 2(a,b)) and a quasi-2D FS with strong $4f$ contributions (Fig. 2(e) and Fig. S8 in [24]) provides direct spectroscopic proof of these key factors. The quantitative information obtained herein lays the basis for more in-depth investigations in the future. Our results may also help explain why the superconducting parity transition, originally proposed in the ideal 2D systems [3], can be realized in bulk CeRh_2As_2 [1] - since the superconductivity is mainly driven by the quasi-2D $4f$ bands from the Ce layers.

In summary, our high-resolution ARPES measurements on CeRh_2As_2 , in combination with DFT+DMFT calculations, demonstrate that the Ce $4f$ electrons play a significant role in the FS due to band-dependent c - f hybridization. We find that the FS exhibits clear nesting at $(\pi/a, \pi/a)$ and the nesting is facilitated by a VHS near \bar{X} at $k_z = \pi/c$, originating from c - f hybridization. The FS nesting can well explain the observed AFM excitations at $(\pi/a, \pi/a)$ from INS measurements [12], which might be the driving force for its superconductivity. Our results further unveil the fine band splittings related to the locally noncentrosymmetric structure, a quasi-2D FS due to weak interlayer hopping and strong Kondo peaks likely caused by low-lying CEF excitations. The spectroscopic insight can be important to understand the electronic and magnetic excitations in CeRh_2As_2 , as well as the origin of multiple superconducting phases in this enigmatic compound.

This work is supported by the National Key R&D Program of China (Grant No. 2022YFA140220, No. 2023YFA1406303), the State Key project of Zhejiang Province (No. LZ22A040007), the National Science Foundation of China (No. 12174331, 12204159, 12274364), the Key R&D Program of Zhejiang Province, China (2021C01002), and the Bridging Grant (BG 11-072020) with China, Japan, South Korea and ASEAN region funded by the Swiss State Secretariat for Education, Research and Innovation. We acknowledge MAX IV Laboratory for time on Beamline BLOCH under Proposal 20200306. Research conducted at MAX IV, a Swedish national user facility, is supported by the Swedish Research council under contract 2018-07152, the Swedish Governmental Agency for Innovation Systems under contract 2018-04969, and Formas under contract 2019-02496. We thank Dr. Craig Polley, Ms. Dongting Zhang, Mr. Yuxin Chen, Dr. Tong Chen, Prof. Yu Song, Prof. Michael Smidman and Prof. Xin Lu for experimental assistance or helpful discussion.

Note: during the submission process of our paper, we became aware of an independent ARPES work on CeRh_2As_2 [47], which emphasizes the coexistence of the VHS near X at $k_z = 0$ and the $4f$ flat bands.

* These authors contributed equally to this paper

† ccao@zju.edu.cn

‡ hqyuan@zju.edu.cn

§ yangliuphys@zju.edu.cn

- [1] S. Khim, J. F. Landaeta, J. Banda, N. Bannor, M. Brando, P. Brydon, D. Hafner, R. K uchler, R. Cardoso-Gil, U. Stockert, A. P. Mackenzie, D. F. Agterberg, C. Geibel, and E. Hassinger, *Field-induced transition within the superconducting state of CeRh_2As_2* , *Science* **373**, 1012 (2021).
- [2] J. F. Landaeta, P. Khanenko, D. C. Cavanagh, C. Geibel, S. Khim, S. Mishra, I. Sheikin, P. M. R. Brydon, D. F. Agterberg, M. Brando, and E. Hassinger, *Field-Angle Dependence Reveals Odd-Parity Superconductivity in CeRh_2As_2* , *Phys. Rev. X* **12**, 031001 (2022).
- [3] T. Yoshida, M. Sigrist, and Y. Yanase, *Pair-density wave states through spin-orbit coupling in multilayer superconductors*, *Phys. Rev. B* **86**, 134514 (2012).
- [4] K. Nogaki, A. Daido, J. Ishizuka, and Y. Yanase, *Topological crystalline superconductivity in locally noncentrosymmetric CeRh_2As_2* , *Phys. Rev. Research* **3**, L032071 (2021).
- [5] D. M ockli and A. Ramires, *Two scenarios for superconductivity in CeRh_2As_2* , *Phys. Rev. Research* **3**, 023204 (2021).
- [6] A. Skurativska, M. Sigrist, and M. H. Fischer, *Spin response and topology of a staggered-Rashba superconductor*, *Phys. Rev. Research* **3**, 033133 (2021).
- [7] D. C. Cavanagh, T. Shishidou, M. Weinert, P. M. R. Brydon, and D. F. Agterberg, *Nonsymmorphic symmetry and field-driven odd-parity pairing in CeRh_2As_2* , *Phys. Rev. B* **105**, L020505 (2022).
- [8] E. G. Schertenleib, M. H. Fischer, and M. Sigrist, *Unusual H - T phase diagram of CeRh_2As_2 : The role of staggered noncentrosymmetry*, *Phys. Rev. Research* **3**, 023179 (2021).
- [9] D. M ockli and A. Ramires, *Superconductivity in disordered locally noncentrosymmetric materials: An application to CeRh_2As_2* , *Phys. Rev. B* **104**, 134517 (2021).
- [10] M. H. Fischer, M. Sigrist, D. F. Agterberg, and Y. Yanase, *Superconductivity and Local Inversion-Symmetry Breaking*, *arXiv preprint arXiv:2204.02449* (2022).
- [11] H. Siddiquee, Z. Rehfuss, C. Broyles, and S. Ran, *Tuning the parity of superconductivity in CeRh_2As_2 via pressure*, *arXiv preprint arXiv:2212.06930v1* (2022).
- [12] T. Chen, H. Siddiquee, Z. Rehfuss, C. Lygouras, J. Drouin, S. Gao, K. E. Avers, C. J. Schmitt, A. Podlesnyak, Y. Song, S. Ran and C. Broholm, *Antiferromagnetic spin fluctuation in the spin-triplet superconductor candidate CeRh_2As_2* , 2024 APS march meeting abstract.
- [13] M. Kibune, S. Kitagawa, K. Kinjo, S. Ogata, M. Manago, T. Taniguchi, K. Ishida, M. Brando, E. Hassinger, H. Rosner, C. Geibel, and S. Khim, *Observation of Antiferromagnetic Order as Odd-Parity Multipoles inside the Superconducting Phase in CeRh_2As_2* , *Phys. Rev. Lett.* **128**, 057002 (2022).
- [14] D. Hafner, P. Khanenko, E.-O. Eljaouhari, R. K uchler, J. Banda, N. Bannor, T. L uhmann, J. F. Landaeta, S. Mishra, I. Sheikin, E. Hassinger, S. Khim, C. Geibel,

- G. Zwirnagl, and M. Brando, *Possible Quadrupole Density Wave in the Superconducting Kondo Lattice CeRh₂As₂*, *Phys. Rev. X* **12**, 011023 (2022).
- [15] F. Steglich, J. Aarts, C. D. Bredl, W. Lieke, D. Meschede, W. Franz, and H. Schäfer, *Superconductivity in the Presence of Strong Pauli Paramagnetism: CeCu₂Si₂*, *Phys. Rev. Lett.* **43**, 1892 (1979).
- [16] M. Smidman, O. Stockert, E. M. Nica, Y. Liu, H. Yuan, Q. Si, and F. Steglich, *Colloquium: Unconventional fully gapped superconductivity in the heavy-fermion metal CeCu₂Si₂*, *Rev. Mod. Phys.* **95**, 031002 (2023).
- [17] C. Petrovic, P. G. Pagliuso, M. F. Hundley, R. Movshovich, J. L. Sarrao, J. D. Thompson, Z. Fisk, and P. Monthoux, *Heavy-fermion superconductivity in CeCoIn₅ at 2.3 K*, *J. Phys.: Condens. Matter* **13**, L337 (2001).
- [18] G. Zwirnagl, *The utility of band theory in strongly correlated electron systems*, *Rep. Prog. Phys.* **79**, 124501 (2016).
- [19] K. Nogaki and Y. Yanase, *Even-odd parity transition in strongly correlated locally noncentrosymmetric superconductors: Application to CeRh₂As₂*, *Phys. Rev. B* **106**, L100504 (2022).
- [20] T. Hazra and P. Coleman, *Triplet pairing mechanisms from Hund's-Kondo models: applications to UTe₂ and CeRh₂As₂*, *Phys. Rev. Lett.* **130**, 136002 (2023).
- [21] K. Machida, *Violation of the Pauli-Clogston limit in a heavy Fermion superconductor CeRh₂As₂ –Duality of itinerant and localized 4f electrons–*, *Phys. Rev. B* **106**, 184508 (2022).
- [22] J. Ishizuka, K. Nogaki, M. Sigrist, and Y. Yanase, *Correlation-induced Fermi surface evolution and topological crystalline superconductivity in CeRh₂As₂ via pressure*, *arXiv preprint arXiv:2311.00324v1* (2023).
- [23] A. Ptok, K. J. Kapcia, P. T. Jochym, J. Łażewski, A. M. Oleś, and P. Piekarczyk, *Electronic and dynamical properties of CeRh₂As₂: Role of Rh₂As₂ layers and expected orbital order*, *Phys. Rev. B* **104**, L041109 (2021).
- [24] See online supplementary material at xxx, which includes Refs.[25-35] and details on crystal growth, characterizations, ARPES measurements and calculations.
- [25] S. Ernst, S. Kirchner, C. Krellner, C. Geibel, G. Zwirnagl, F. Steglich, and S. Wirth, *Emerging local Kondo screening and spatial coherence in the heavy-fermion metal YbRh₂Si₂*, *Nature* **474**, 362 (2011).
- [26] S. Wirth and F. Steglich, *Exploring heavy fermions from macroscopic to microscopic length scales*, *Nat. Rev. Mater.* **1**, 16051 (2016).
- [27] S.-i. Kimura, J. Sichelschmidt, and S. Khim, *Optical study of the electronic structure of locally noncentrosymmetric CeRh₂As₂*, *Phys. Rev. B* **104**, 245116 (2021).
- [28] G. Kresse and J. Hafner, *Ab initio molecular dynamics for liquid metals*, *Phys. Rev. B* **47**, 558 (1993).
- [29] G. Kresse and D. Joubert, *From ultrasoft pseudopotentials to the projector augmented-wave method*, *Phys. Rev. B* **59**, 1758 (1999).
- [30] J. P. Perdew, K. Burke, and M. Ernzerhof, *Generalized Gradient Approximation Made Simple*, *Phys. Rev. Lett.* **77**, 3865 (1996).
- [31] A. A. Mostofi, J. R. Yates, Y.-S. Lee, I. Souza, D. Vanderbilt, and N. Marzari, *wannier90: A tool for obtaining maximally-localised Wannier functions*, *Computer Physics Communications* **178**, 685 (2008).
- [32] G.-X. Zhi, C.-C. Xu, S.-Q. Wu, F.-L. Ning, and C. Cao, *WannSymm: A symmetry analysis code for Wannier orbitals*, *Computer Physics Communications* **271**, 108916 (2022).
- [33] K. Haule, C.-H. Yee, and K. Kim, *Dynamical mean-field theory within the full-potential methods: electronic structure of CeIrIn₅, CeCoIn₅ and CeRhIn₅*, *Phys. Rev. B* **81**, 195107 (2010).
- [34] K. Schwarz, P. Blaha, and G. K. H. Madsen, *Electronic structure calculations of solids using the WIEN2k package for material sciences*, *Computer Physics Communications* **147**, 71 (2002).
- [35] K. Haule, *Quantum Monte Carlo impurity solver for cluster dynamical mean-field theory and electronic structure calculations with adjustable cluster base*, *Phys. Rev. B* **75**, 155113 (2007).
- [36] J. D. Denlinger, G.-H. Gweon, J. W. Allen, C. G. Olson, M. B. Maple, J. Sarrao, P. Armstrong, Z. Fisk, and H. Yamagami, *Comparative study of the electronic structure of XRu₂Si₂: probing the Anderson lattice*, *Journal of Electron Spectroscopy and Related Phenomena* **117**, 347 (2001).
- [37] Z. Wu, Y. Fang, H. Su, W. Xie, P. Li, Y. Wu, Y. Huang, D. Shen, B. Thiagarajan, J. Adell, C. Cao, H.-Q. Yuan, F. Steglich, and Y. Liu, *Revealing the heavy quasiparticles in the heavy-fermion superconductor CeCu₂Si₂*, *Phys. Rev. Lett.* **127**, 067002 (2021).
- [38] A. Sekiyama, T. Iwasaki, K. Matsuda, Y. Saitoh, Y. Ônuki, and S. Suga, *Probing bulk states of correlated electron systems by high-resolution resonance photoemission*, *Nature* **403**, 396 (2000).
- [39] J. W. Allen, *The Kondo resonance in electron spectroscopy*, *Journal of the Physical Society of Japan* **74**, 34 (2005).
- [40] S.-i. Fujimori, *Band structures of 4f and 5f materials studied by angle-resolved photoelectron spectroscopy*, *Journal of Physics: Condensed Matter* **28**, 153002 (2016).
- [41] H. J. Im, T. Ito, H.-D. Kim, S. Kimura, K. E. Lee, J. B. Hong, Y. S. Kwon, A. Yasui, and H. Yamagami, *Direct Observation of Dispersive Kondo Resonance Peaks in a Heavy-Fermion System*, *Phys. Rev. Lett.* **100**, 176402 (2008).
- [42] Q. Y. Chen, D. F. Xu, X. H. Niu, J. Jiang, R. Peng, H. C. Xu, C. H. P. Wen, Z. F. Ding, K. Huang, L. Shu, Y. J. Zhang, H. Lee, V. N. Strocov, M. Shi, F. Bisti, T. Schmitt, Y. B. Huang, P. Dudin, X. C. Lai, S. Kirchner, H. Q. Yuan, and D. L. Feng, *Direct observation of how the heavy-fermion state develops in CeCoIn₅*, *Phys. Rev. B* **96**, 045107 (2017).
- [43] S. Y. Jang, J. D. Denlinger, J. W. Allen, V. S. Zapf, M. B. Maple, J. N. Kim, B. G. Jang, and J. H. Shim, *Evolution of the Kondo lattice electronic structure above the transport coherence temperature*, *Proc. Natl. Acad. Sci.* **117**, 23467 (2020).
- [44] S. Kirchner, S. Paschen, Q. Chen, S. Wirth, D. Feng, J. D. Thompson, and Q. Si, *Colloquium: Heavy-electron quantum criticality and single-particle spectroscopy*, *Rev. Mod. Phys.* **92**, 011002 (2020).
- [45] Y. Wu, Y. Zhang, F. Du, B. Shen, H. Zheng, Y. Fang, M. Smidman, C. Cao, F. Steglich, H. Yuan, J. D. Denlinger, and Y. Liu, *Anisotropic c – f Hybridization in the Ferromagnetic Quantum Critical Metal CeRh₆Ge₄*, *Phys. Rev. Lett.* **126**, 216406 (2021).
- [46] Y.-H. Yuan, Y.-X. Duan, J. Ruzs, C. Zhang, J.-J. Song,

- Q.-Y. Wu, Y. Sassa, O. Tjernberg, M. Månsson, M. H. Berntsen, F.-Y. Wu, S.-Y. Liu, H. Liu, S.-X. Zhu, Z.-T. Liu, Y.-Z. Zhao, P. H. Tobash, E. D. Bauer, J. D. Thompson, P. M. Oppeneer, T. Durakiewicz, and J.-Q. Meng, *Angle-resolved photoemission spectroscopy view on the nature of Ce 4f electrons in the antiferromagnetic Kondo lattice CePd₅Al₂*, *Phys. Rev. B* **103**, 125122 (2021).
- [47] X. Chen, L. Wang, J. Ishizuka, K. Nogaki, Y. Cheng, F. Yang, R. Zhang, Z. Chen, F. Zhu, Y. Yanase, B. Lv, and Y. Huang, *Coexistence of near- E_F flat band and van Hove singularity in a two-phase superconductor*, *arXiv preprint arXiv:2309.05895v1* (2023).
- [48] A. S. Cameron, G. Friemel, and D. S. Insovo, *Multipolar phases and magnetically hidden order: review of the heavy-fermion compound Ce_{1-x}La_xB₆*, *Rep. Prog. Phys.* **79**, 066502 (2016).
- [49] A. Koitzsch, N. Heming, M. Künzler, B. Büchner, P. Y. Portnichenko, A. V. Dukhnenko, N. Y. Shitsevalova, V. B. Filipov, L. L. Lev, V. N. Strocov, J. Ollivier, and D. S. Inosov, *Nesting-driven multipolar order in CeB₆*, *Nat. Commun.* **7**, 10876 (2016).
- [50] D. Jang, P. Y. Portnichenko, A. S. Cameron, G. Friemel, A. V. Dukhnenko, N. Y. Shitsevalova, V. B. Filipov, A. Schneidewind, A. Ivanov, D. S. Inosov, and M. Brando, *Large positive correlation between the effective electron mass and the multipolar fluctuation in the heavy-fermion metals Ce_{1-x}La_xB₆*, *npj Quantum Materials* **2**, 62 (2017).
- [51] Q. Y. Chen, C. H. P. Wen, Q. Yao, K. Huang, Z. F. Ding, L. Shu, X. H. Niu, Y. Zhang, X. C. Lai, Y. B. Huang, G. B. Zhang, S. Kirchner, and D. L. Feng, *Tracing crystal-field splittings in the rare-earth-based intermetallic CeIrIn₅*, *Phys. Rev. B* **97**, 075149 (2018).
- [52] D. Ehm, S. Hüfner, F. Reinert, J. Kroha, P. Wölfle, O. Stockert, C. Geibel, and H. v. Löhneysen, *High-resolution photoemission study on low- T_K Ce systems: Kondo resonance, crystal field structures, and their temperature dependence*, *Phys. Rev. B* **76**, 045117 (2007).
- [53] S. Patil, A. Generalov, M. Güttler, P. Kushwaha, A. Chikina, K. Kummer, T. C. Rödel, A. F. Santander-Syro, N. Caroca-Canales, C. Geibel, S. Danzenbächer, Y. Kucherenko, C. Laubschat, J. W. Allen, and D. V. Vyalikh, *ARPES view on surface and bulk hybridization phenomena in the antiferromagnetic Kondo lattice CeRh₂Si₂*, *Nat. Commun.* **7**, 11029 (2016).
- [54] D. S. Christovam, M. Ferreira-Varvalho, A. Marino, M. Sunderman, D. Takegami, K. D. Melendez-Sans, Anna annnd Tsuei, Z. Hu, S. Rößler, M. Valvidares, M. W. Haverkort, Y. Liu, E. D. Bauer, L. H. Tjeng, G. Zwicknagl, and A. Severing, *Spectroscopic evidence of Kondo-induced quasi-quartet in CeRh₂As₂ via pressure*, *arXiv preprint arXiv:2308.10063v1* (2023).
- [55] K. McElroy, G.-H. Gweon, S. Y. Zhou, J. Graf, S. Uchida, H. Eisaki, H. Takagi, T. Sasagawa, D.-H. Lee, and A. Lanzara, *Elastic Scattering Susceptibility of the High Temperature Superconductor Bi₂Sr₂CaCu₂O_{8+ δ} : A Comparison between Real and Momentum Space Photoemission Spectroscopies*, *Phys. Rev. Lett.* **96**, 067005 (2006).
- [56] U. Chatterjee, M. Shi, A. Kaminski, A. Kanigel, H. M. Fretwell, K. Terashima, T. Takahashi, S. Rosenkranz, Z. Z. Li, H. Raffy, A. Santander-Syro, K. Kadowaki, M. R. Norman, M. Randeria, and J. C. Campuzano, *Nondispersive Fermi Arcs and the Absence of Charge Ordering in the Pseudogap Phase of Bi₂Sr₂CaCu₂O_{8+ δ}* , *Phys. Rev. Lett.* **96**, 107006 (2006).
- [57] D. W. Shen, B. P. Xie, J. F. Zhao, L. X. Yang, L. Fang, J. Shi, R. H. He, D. H. Lu, H. H. Wen, and D. L. Feng, *Novel Mechanism of a Charge Density Wave in a Transition Metal Dichalcogenide*, *Phys. Rev. Lett.* **99**, 216404 (2007).
- [58] I. Eremin, G. Zwicknagl, P. Thalmeier, and P. Fulde, *Feedback Spin Resonance in Superconducting CeCu₂Si₂ and CeCoIn₅*, *Phys. Rev. Lett.* **101**, 187001 (2008).
- [59] O. Stockert, J. Arndt, E. Faulhaber, C. Geibel, H. S. Jeevan, S. Kirchner, M. Loewenhaupt, K. Schmalzl, W. Schmidt, Q. Si, and F. Steglich, *Magnetically driven superconductivity in CeCu₂Si₂*, *Nat. Phys.* **7**, 119 (2011).
- [60] N. K. Sato, N. Aso, K. Miyake, R. Shiina, P. Thalmeier, G. Varelogiannis, C. Geibel, F. Steglich, P. Fulde, and Komatsubara, *Strong coupling between local moments and superconducting 'heavy' electrons in UPd₂Al₃*, *Nature* **410**, 340 (2001).
- [61] O. Stockert and F. Steglich, *Spin resonances in heavy-fermion superconductors*, *Physica C: Superconductivity and its Applications* **615**, 1354375 (2023).
- [62] J. A. Mydosh and P. M. Oppeneer, *Hidden order, superconductivity, and magnetism: The unsolved case of URu₂Si₂*, *Rev. Mod. Phys.* **83**, 1301 (2011).
- [63] H. Ikeda, M.-T. Suzuki, R. Arita, T. Takimoto, T. Shibauchi, and Y. Matsuda, *Emergent rank-5 nematic order in URu₂Si₂*, *Nat. Phys.* **8**, 528 (2012).
- [64] C. Broholm, J. K. Kjems, W. J. L. Buyers, P. Matthews, T. T. M. Palstra, A. A. Menovsky, and J. A. Mydosh, *Magnetic Excitations and ordering in the Heavy-Electron Superconductor URu₂Si₂*, *Phys. Rev. Lett.* **58**, 1467 (1987).
- [65] C. Broholm, H. Lin, P. T. Matthews, T. E. Mason, W. J. L. Buyers, M. F. Collins, A. A. Menovsky, J. A. Mydosh, and J. K. Kjems, *Magnetic excitations in the heavy-fermion superconductor URu₂Si₂*, *Phys. Rev. B* **43**, 12809 (1991).
- [66] C. R. Wiebe, J. A. Janik, G. J. MacDougall, G. M. Luke, J. D. Garrett, H. D. Zhou, Y.-J. Jo, L. Balicas, Y. Qiu, J. R. D. Copley, Z. Yamani, and W. J. L. Buyers, *Gapped itinerant spin excitations account for missing entropy in the hidden-order state of URu₂Si₂*, *Nat. Phys.* **3**, 96 (2007).
- [67] A. F. Santander-Syro, M. Klein, F. L. Boariu, A. Nuber, P. Lejay, and F. Reinert, *Fermi-surface instability at the 'hidden-order' transition of URu₂Si₂*, *Nat. Phys.* **5**, 637 (2009).
- [68] F. L. Boariu, C. Bareille, H. Schwab, A. Nuber, P. Lejay, T. Durakiewicz, F. Reinert, and A. F. Santander-Syro, *Momentum-resolved evolution of the Kondo lattice into "hidden order" in URu₂Si₂*, *Phys. Rev. Lett.* **110**, 156404 (2013).
- [69] S. Chatterjee, J. Trinckauf, T. Hänke, D. E. Shai, J. W. Harter, T. J. Williams, G. M. Luke, K. M. Shen, and J. Geck, *Formation of the coherent heavy fermion liquid at the hidden order transition in URu₂Si₂*, *Phys. Rev. Lett.* **110**, 186401 (2013).
- [70] J.-Q. Meng, P. M. Oppeneer, J. A. Mydosh, P. S. Riseborough, K. Gofryk, J. J. Joyce, E. D. Bauer, Y. Li, and T. Durakiewicz, *Imaging the three-dimensional Fermi-surface pairing near the hidden-order transition in URu₂Si₂ using angle-resolved photoemission spec-*

- troscopy*, *Phys. Rev. Lett.* **111**, 127002 (2013).
- [71] R. Yoshida, Y. Nakamura, M. Fukui, Y. Haga, E. Yamamoto, Y. Ônuki, M. Okawa, S. Shin, M. Hirai, Y. Muiraoka, and T. Yokoya, *Signature of hidden order and evidence of periodicity modification in URu₂Si₂*, *Phys. Rev. B* **82**, 205108 (2010).
- [72] W. Zhang, H. Y. Lu, D. H. Xie, W. Feng, S. Y. Tan, Y. Liu, X. G. Zhu, Y. Zhang, Q. Q. Hao, Y. B. Huang, X. C. Lai, and Q. Y. Chen, *ARPES/STM study of the surface terminations and 5f-electron character in URu₂Si₂*, *Phys. Rev. B* **98**, 115121 (2018).
- [73] J. D. Denlinger, J.-S. Kang, L. Dudy, J. W. Allen, K. Kim, J.-H. Shim, K. Haule, J. L. Sarrao, N. P. Butch, and M. B. Maple, *Global perspectives of the bulk electronic structure of URu₂Si₂ from angle-resolved photoemission*, *Electron. Struct.* **4**, 013001 (2022).
- [74] S. Mishra, Y. Liu, E. D. Bauer, F. Ronning, and S. M. Thomas, *Anisotropic magnetotransport properties of the heavy-fermion superconductor CeRh₂As₂*, *Phys. Rev. B* **106**, L140502 (2022).